Observation of peat porosity and water retention upon drying

Parra-Gómez, Luis J.; Jommi, Cristina; Muraro, Stefano

DOI
10.1051/e3sconf/202564203027

Publication date
2025

Document Version
Final published version

Published in
E3S Web of Conferences

Observation of peat porosity and water retention upon drying

Luis J. Parra-Gómez[1,*], *Cristina* Jommi[1,2], and *Stefano* Muraro[1]

[1] Delft University of Technology, Department of Geosciences and Engineering, Stevinweg 1 2628CN Delft, The Netherlands
[2] Politecnico di Milano, Department of Civil and Environmental Engineering, piazza Leonardo da Vinci 32 20133 Milano, Italy

Abstract. Peat is a highly organic material that poses significant environmental and geotechnical engineering challenges due to its hydrological relevance and atypical mechanical behaviour. Understanding its unsaturated response is essential for infrastructure built over organic soils, particularly under increasing seasonal variability associated with increased climate stresses. Modelling the water retention behaviour of peat remains complex due to its high compressibility and the fabric rearrangements induced by drying and wetting cycles. This study presents an experimental characterisation of the shrinkage and water retention behaviour of natural and reconstituted fibrous peat from the Netherlands. A combination of high-resolution laser scanning and suction measurements was employed to monitor volume change and water retention throughout drying. The results are interpreted through a framework that distinguishes between inter- and intra-ped porosities, allowing for the separation of their respective contributions to shrinkage and retention. Complementary mercury intrusion porosimetry (MIP) analyses provided insight into the evolution of pore size distribution during drying, supporting the interpretation of a sequential engagement of pore sizes. The findings underscore the importance of accounting for differential multiscale porosity evolution and fabric structure when evaluating the hydro-mechanical response of peat.

1. Introduction

Histosols, including peat, cover approximately 2.8% of the global land surface and play a significant role as carbon sinks, providers of ecosystem services, and regulators of hydrological conditions [1]. At the same time, peat soils present considerable challenges for infrastructure development and maintenance. In the Netherlands, for example, approximately 3,500 km of regional dykes are constructed on peat and require regular inspection and maintenance to ensure their stability and performance [2].

The stability of peat deposits is increasingly affected by climate stresses, particularly rising temperatures and the associated intensification of extreme rainfall and drought events. More frequent and severe wetting-drying cycles expose organic material to oxygen, accelerating subsidence and increasing CO_2 emissions. Besides environmental concerns, these processes may have implications on the safety and serviceability of peat-based infrastructure, as they can lead to seasonal deformations, cracking, and progressive material degradation [3].

Peat is an organic soil with an organic matter content exceeding 80% and porosity above 90%, characterised by a highly structured fabric composed of a multiscale arrangement of organic fibres [4,5]. Its most distinctive mechanical property is high compressibility, which results in volumetric reductions of up to 70% during drying [6]. The water retention and shrinkage/swelling behaviour of peat has been examined independently across soil science, agriculture, and engineering disciplines [7-12]. Most studies adopt a phenomenological approach, rarely linking the observed shrinkage to the water retention. Few investigations have explicitly addressed how the complex porous structure of peat influences its hydraulic response [13-17] .

Parra-Gómez et al. [18] recently proposed a framework that relates shrinkage and water retention to the evolution of the pore size distribution. However, this approach remains unvalidated due to lack of direct experimental evidence on the evolution of porosity during drying. The present study provides experimental data to substantiate this pore-centric framework further and to discuss the evolution of porosity upon drying.

2. Experimental characterisation

An experimental campaign was conducted to examine the relationship between porosity, shrinkage, and water retention in peat. The study was conducted on peat retrieved from a depth of 2.5 meters at the Leendert de Boerspolder site in the Netherlands.

A block of natural peat sample was recovered with a water content w_c around 695%, an initial void ratio, e_0 of 10.15 and a specific gravity G_s of 1.50. The loss on ignition, LOI was measured between 80% and 90%, while the gravimetric fibre content FC ranged from 15% to 24% [19-21].

Assessment of the sample fabric was carried out using environmental scanning electron microscopy (ESEM). Imaging revealed a highly structured peat fabric

* Corresponding author: L.J.Parragomez@tudelft.nl

consisting of a multiscale arrangement of organic fibres, and seldom to no presence of mineral particles. The peat composition appears to be formed by fibrous organic structures where bigger fibres can be observed to be embedded in ped-like aggregations or tangles of smaller fibres with high intra-ped porosity, and separated by larger inter-ped voids (see Fig. 1).

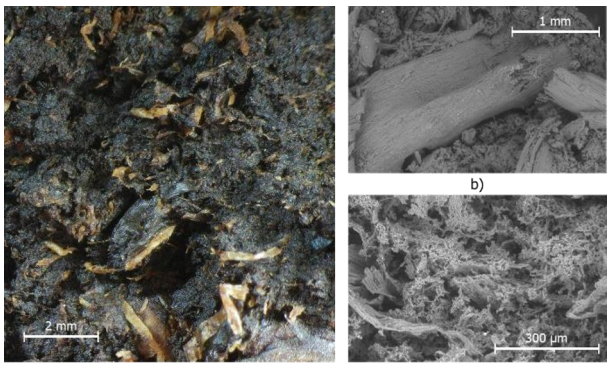

Fig. 1. Observations of peat fabric. a) Optical microscope; b) Fibres and peds in the ESEM; c) Inner structure of organic peds.

A reconstituted peat sample was prepared from the same material by disaggregating the peat and mixing it into a slurry with a water content of approximately 850%. The slurry was then oedometrically consolidated under a vertical effective stress of 30 kPa, consistent with the measured pre-consolidation pressure at the site. The reconstituted sample developed a denser and more homogeneous structure, due to the reduced inter-ped porosity caused by the reconstitution process. Four natural (Nat) and reconstituted (Rec) peat samples were subjected to wetting and drying cycles while monitoring their soil shrinkage curve (SSC) and soil water retention (SWR). Before the start of the test, samples were allowed to saturate for 24 hours by capillary rise. Table 1 summarises the sample properties at the onset of drying.

Table 1. Sample initial properties.

Sample	Test	w_c (%)	γ_t (kN/m³)	G_s (-)	e_0 (-)	S_r (-)
Nat	SWR	682	10.27	1.507	10.48	0.98
	SSC	702	10.10	1.486	10.58	0.99
Rec	SWR	459	10.49	1.498	6.826	1.00
	SSC	457	10.36	1.498	6.895	0.99

2.1. Soil shrinkage curve (SSC)

Shrinkage measurements were performed on 38 mm cylindrical samples with a 1:1 height to diameter ratio. Upon drying, the samples underwent significant volume changes and non-uniform deformation, which distorted the initial cylindrical shape of the material. The volume change of the samples was monitored using a three-dimensional system of laser distance sensors with an accuracy of 10 µm, mounted on motorised rails with a location accuracy of 0.02 mm around a revolving stage with an angular precision of 0.45°. Scans with the laser array enable the reconstruction of a point cloud of the sample surface, comprising approximately 1500 points. The point cloud was then smoothed into a continuous surface using a Gaussian kernel defined in spherical coordinates, and the internal surface volume was calculated by numerical integration. The water content of the sample was tracked by measuring its weight before and after each laser scan. Fig. 2 shows a schematic of the laser system and an example of its output.

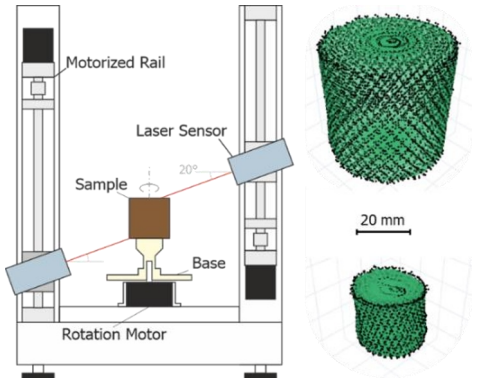

Fig. 2. Schematic of the 3D laser scanner and example of results at the beginning and at the end of shrinkage.

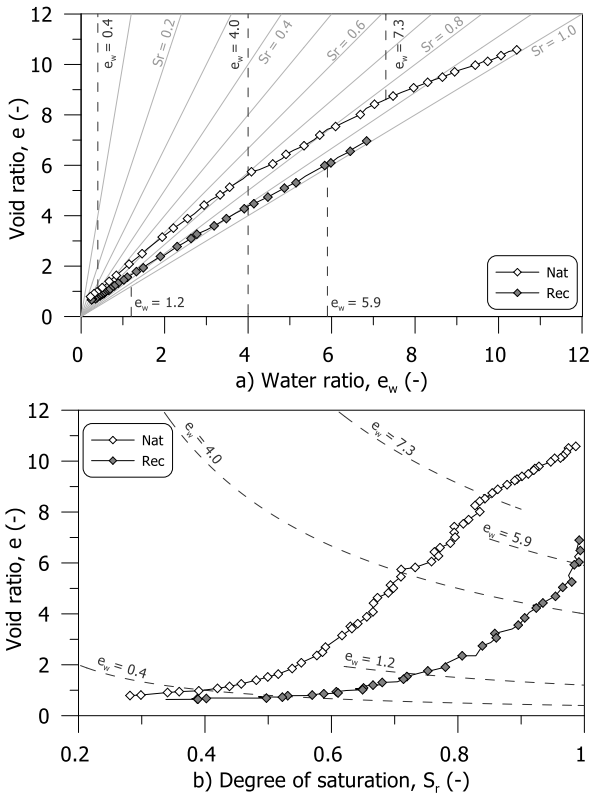

Fig. 3. Soil shrinkage curves obtained for the tested peat samples: a) water ratio domain; b) saturation domain.

Fig. 3 shows the soil shrinkage behaviour of both samples in the water ratio ($e_w = G_s w_c$) and saturation domains. If the change of water volume in the sample is linearised around the current configuration as a proportion of the total change of volume, such that $\Delta e_w = k\Delta e$, then the relationship between the sample void ratio and saturation depends on the initial void ratio e_0 and initial saturation S_{r0} and follows the hyperbolic relation in Eq. 1.

$$e = e_0 \frac{k - S_{r0}}{k - S_r} \quad (1)$$

The equation provides a means to distinguish between shrinkage stages by fitting the experimental data to obtain the k coefficient. When k is greater than 1, the sample loses more water than volume, which implies desaturation-driven shrinkage. A value of k equal to 1 implies proportional shrinkage, and a value of k smaller than 1 implies that the sample loses more volume than water, suggesting a possible collapse of the soil structure, here referred to as accelerated shrinkage. Accounting for experimental error, a range of k between 0.95 and 1.05 was taken as indicative of proportional shrinkage.

The natural and reconstituted samples exhibited markedly different shrinkage behaviours. The natural sample followed a shrinkage sequence with four steps consistent with observations reported in the literature [7,18]. An initial stage of desaturation-driven shrinkage was observed up to a water ratio of 7.3, characterised by a coefficient k of 1.63, during which saturation decreased steadily. This was followed by a stage of proportional shrinkage extending to a water ratio of 4.0, with k of 1.05, where the incremental reduction in water volume almost matched the reduction in sample volume, reducing the rate of desaturation. Subsequently, the sample entered a phase of accelerated shrinkage, up to a water ratio of 0.4, with k=0.77, which eventually slowed down as the sample approached residual conditions.

The reconstituted sample followed a sequence more closely aligned with proportional shrinkage, with k=1.00 up to a water ratio of 5.9. This was followed by a brief phase of desaturation-driven shrinkage, k=1.15, extending to a water ratio of 4.0. A second proportional stage, with k =1.02, continued until a water ratio of 1.2, after which a slightly accelerated phase was observed, with k=0.90, extending to 0.4. As in the natural sample, shrinkage then decelerated as the sample approached residual conditions.

The strong differences between samples suggest a strong dependence of soil shrinkage on the initial soil fabric. Particularly, it suggests that the proportion of large inter-ped or fibre-associated pores of the sample is directly linked to the amount of desaturation-driven shrinkage experienced by the sample. These are less prevalent in the homogeneous and massive fabric of the reconstituted sample, which showed a more proportional shrinkage. Given its homogeneous deformation, the response of the reconstituted sample may be considered representative of the mechanical response of the peds.

By assuming that the Cartesian coordinates (x, y, z) correspond to the principal strain directions during drying, the deviatoric strain can be calculated according to Eq. 2. With the deviatoric and volumetric strains, the strain anisotropy angle β was computed according to Eq. 3, and its evolution with the water ratio is shown in Fig. 4. Both samples exhibit a highly anisotropic response at the beginning of drying, which becomes incrementally isotropic after a water ratio of around 4.0 where the accelerated shrinkage begins. Previous studies have linked this evolution of anisotropy to the engagement of different levels of porosity [17]. The response is present in both samples, suggesting that rather than the transition being governed by the engagement of inter- and intra-ped pores at different levels of drying, the anisotropy may be linked to the previous strain history of the material and the fibre orientation that it induces.

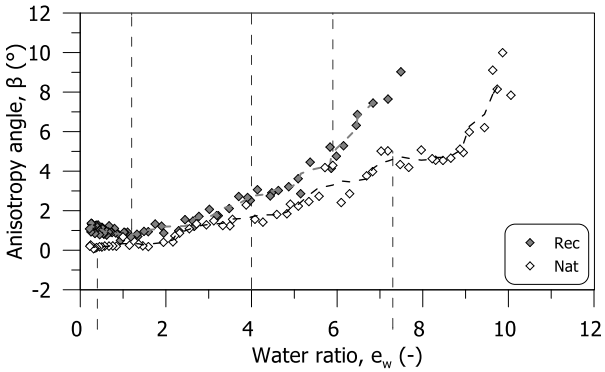

Fig. 4. Change of strain anisotropy with water ratio.

$$\varepsilon_q = \sqrt{\frac{1}{3}[(\varepsilon_x - \varepsilon_y)^2 + (\varepsilon_y - \varepsilon_z)^2 + (\varepsilon_x - \varepsilon_z)^2]} \quad (2)$$

$$\beta = \arctan\left(\frac{\varepsilon_q}{\varepsilon_v}\right) \quad (3)$$

2.1. Soil water retention (SWR)

Cylindrical samples, 70 mm in diameter and height, were used to determine water retention properties using a Hyprop 2 and a WP4C apparatus [22-23]. Measurements were conducted following the drying and wetting procedure described by Parra-Gómez et al. [18], with wetting performed at suction levels of 40 kPa and 70 kPa for the natural sample and 70 kPa for the reconstituted one. The sample drying was conducted inside a small climate chamber at a controlled temperature of 20°C and relative humidity of 40%. The samples were exposed to drying and periodically closed to allow for water redistribution and homogenisation. The overall saturation of the samples could be computed by using the water ratio to associate the corresponding void ratio of the shrinkage test to each suction measurement.

Fig. 5 shows the measured water retention for both samples in the water ratio and suction domains, using the points recorded after reaching a steady state.

The water retention results indicate a similar response between the two samples, with the natural one developing higher suctions than the reconstituted sample (Fig. 5a). Both curves converge at suction values of around 10 MPa. The effects of the different shrinkage curves become evident in the saturation domain (Fig. 5b), where the reconstituted sample has an air entry value that is one order of magnitude higher than that of the natural sample. However, the curves differ significantly up to high suction levels, essentially following the differences in shrinkage.

2.2. Mercury intrusion porosimetry (MIP)

To assess the evolution of porosity throughout drying, the pore size distribution of natural peat samples dried to controlled levels was probed using mercury intrusion

porosimetry. Cylinders with 20 mm diameter and height were dried under the same environmental conditions as the shrinkage and retention tests, while periodically measuring their water ratio and void ratio. One sample was tested in natural conditions, and three other samples were dried until they reached void ratios of 7.5, 5.2 and 2.1, respectively. Table 2 summarises the sample properties, and the corresponding points on the retention curve are shown in Fig. 5a.

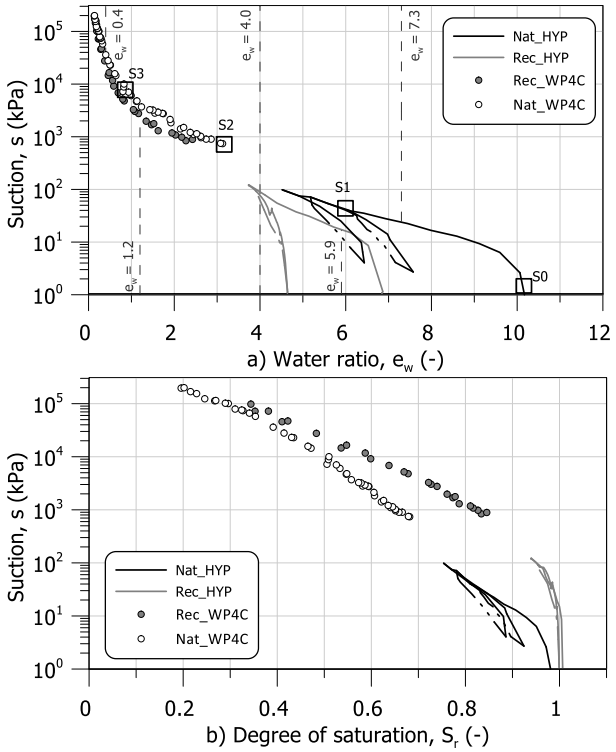

Fig. 5. Soil water retention curves obtained for the tested peat samples: a) water ratio domain; b) saturation domain.

Table 2. Properties of samples tested with MIP: W_d denotes the sample dry weight in grams; n, n_i and n_f denote the total calculated porosity, the intruded porosity and the porosity lost during the initial fill.

ID	e	e_w	$W_d{}^*$	n	n_i	n_f
S0	10.09	10.02	0.142	0.910	0.652	0.230
S1	7.53	6.02	0.172	0.883	0.566	0.324
S2	5.26	3.27	0.274	0.850	0.509	0.343
S3	2.11	0.96	0.656	0.679	0.253	0.427

After reaching the desired void ratio and water content, the samples were flash-frozen using liquid nitrogen at -196°C, broken into pieces with a volume of approximately 1 mL, and freeze-dried by sublimating the ice over 48 hours under a vacuum of 0.1 mbar and a collector temperature differential of 60°C. The fully dry samples were tested in a Micrometrics Autopore IV apparatus at 14°C, and the results were interpreted using a surface tension of 0.484 N/m and a contact angle of 130°, as adopted by Yamaguchi (1992) [24].

Fig. 6 shows the measured cumulative intrusion volume per gram of sample and the corresponding pore size distribution for each of the tested specimens. For comparison, data from an oven-dried sample is included in the plot. It can be seen that the order of magnitude of the total intruded volume per gram of material measured in this study is many times higher than that of the oven-dried sample and consistent with values for peat reported in the literature [25]. The total intruded volume decreases with drying in a manner consistent with the macroscopic shrinkage. However, the effect is not homothetic and appears to affect distinct pore sizes at different stages.

The pore size distribution indicates that, between the natural state (S0) and a void ratio of 7.5 (S1), drying results in the preferential reduction of pores larger than 5 µm, while smaller pores remain largely unaffected. This decrease in macroporosity is accompanied by an apparent increase in pores around 100 µm, which may be attributed to the formation of cracks or the presence of initially occluded pores in the fresh sample. Further drying to a void ratio of 5.2 (S2) primarily affects pores in the 0.4 µm to 5 µm range. The reduction of these intermediate pores results in a double-porosity structure with peaks at 0.8 µm and 40 µm, with the larger pores relatively stable. At a void ratio of 2.0 (S3), most pores smaller than 5 µm and larger than 100 µm are no longer observed, and the resulting pore size distribution becomes comparable to that of an oven-dried sample (OD). The observed sequence of pore shrinkage is consistent with the sequential evacuation described by Parra-Gómez et al. (2023) [18], however, the measured pore sizes are generally larger than those considered in the model.

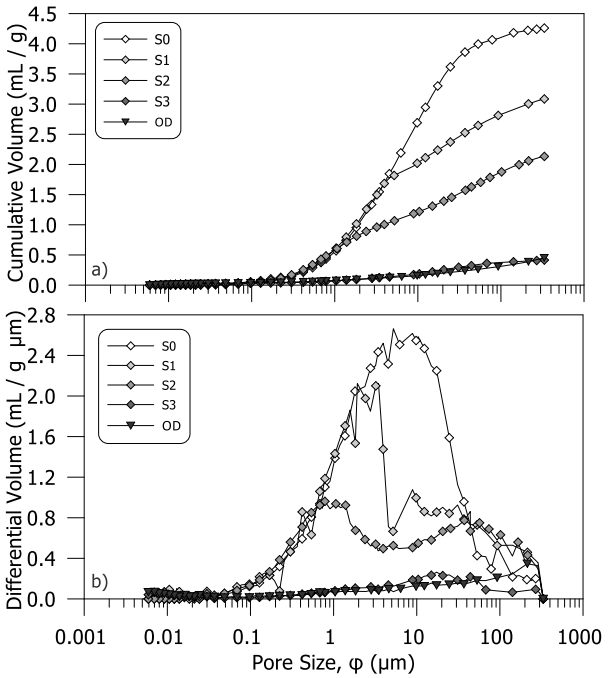

Fig. 6. Evolution of the pore size distribution during drying: a) cumulative volume; b) differential volume.

The mercury intrusion results were assessed by comparing the total porosity, estimated from measurements of unit weight, water content, and specific gravity, with the intruded porosity recorded by the porosimeter. In all cases, the intruded volume was smaller than the estimated porosity, indicating that the analysis did not detect a fraction of the pore space. A filling pressure of 3.4 kPa was applied during the initial stage to ensure complete contact with the penetrometer. At this pressure, larger pores within the sample may be filled and

not detected by the device. Measurements of the penetrometer mass before and after low-pressure mercury filling confirmed that the discrepancy corresponds to porosity lost during the initial filling stage, indicating the presence of pores exceeding 300 µm in diameter. This observation could explain the decreasing proportion of intruded volume with increasing degrees of drying. As samples become drier, the relative proportion of pores larger than 50 µm increases, due to the stability of the macropores and the possible development of cracks.

3. Discussion

The results of the experimental campaign reveal a clear relationship between soil shrinkage, water retention, and changes in porosity. Comparison between the reconstituted and natural sample suggests that the initial desaturation-driven shrinkage of the sample is linked to the larger inter-ped pores being vacated while losing little volume. If the macroscopic retention and shrinkage response of the reconstituted sample is taken as representative of the organic peds, results of both tests can be used to separate the overall void and water ratios into their inter-ped (e^M, e_w^M) and intra-ped (e^m, e_w^m) components. For a given suction level, the total and intra-ped water ratios (e_w, e_w^m) can be determined from the main drying retention curves of the natural and reconstituted samples, respectively. The water ratios can then be used to determine the corresponding (e, e^m) from their respective SSCs. The inter-ped water ratio e_w^M and void ratio e^M, are then determined by subtraction.

Fig. 7a illustrates the soil shrinkage curve, split into its two components, using the total water ratio as a reference. It can be seen that the transitions between desaturation-driven, proportional and accelerated shrinkage seem to be related to changes in the volume of inter-ped pores. The desaturation-driven stage can be mainly attributed to the desaturation of the inter-ped pores, which remain relatively stable at an inter-ped void ratio around 3.0 up to a total water ratio of 7.3. This becomes clearer in Fig. 7b where in the initial desaturation-driven shrinkage, the inter-ped pore space desaturates and converges towards the total shrinkage curve. As seen in Fig. 7c, the saturation drops to a value around 40% without a significant reduction in the inter-ped void ratio.

In the subsequent proportional shrinkage, both porosities shrink at a similar rate until a total water ratio of 4.0, when the shrinkage rate of the intra-ped pores increases (Fig. 7a). The latter may be the reason for the accelerated shrinkage stage. At this point, the shrinkage rate of the inter-ped pores appears to remain fairly constant down to a water ratio of 2.0; afterwards, the rate becomes similar to that of the intra-ped porosity. Fig. 7c shows that after the initial desaturation, the inter-ped porosity is reduced at almost constant saturation. These observations seem to support the interpretation of the accelerated shrinkage being driven by a collapse of the inter-ped contact network [18].

The MIP results show a different pore shrinking sequence with macropores (> 5 µm) being reduced first, and micropores engaging only at higher levels of drying. However, it is worth noting that the sample scale and measuring range of the MIP porosimeter do not account for pores larger than 300 µm. Thus, MIP results may be skewed in favour of showing the behaviour of the intra-ped voids.

The initial constant rate of shrinkage can be explained by the shrinkage progressively impacting from larger to smaller pores. The larger pores decrease first between S0 and S1, but their volume remains stable between S1 and S2 (Fig. 6b), where the microporosity begins to decrease. The sum of both components appears to maintain a relatively constant overall rate of shrinkage until the accelerated stage is reached at a water ratio of 4.0. At this point (S2 to S3), most of the porosity is rapidly reduced at all sizes, explaining the acceleration of the intra-ped shrinkage, which is further exacerbated by the simultaneous collapse of the inter-ped pores.

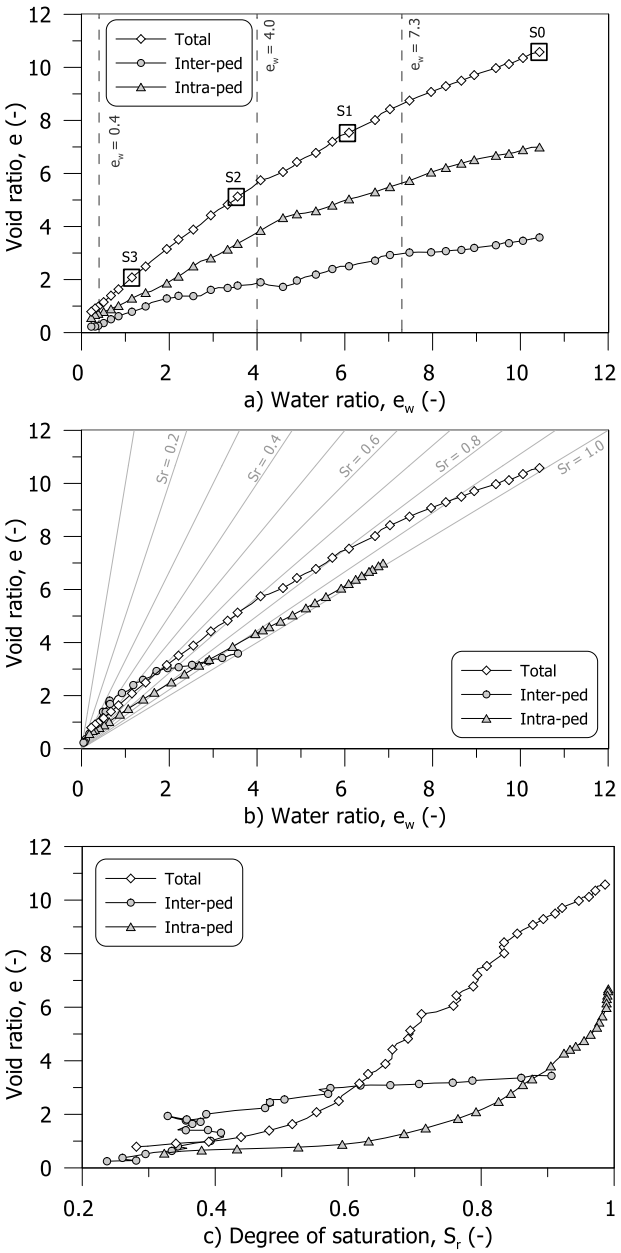

Fig. 7. Natural peat shrinkage curve split into inter- and intra-ped components: a) void ratios with respect to the total water

ratio; b) void ratios with respect to individual water ratios; c) void ratios with respect to individual degree of saturation.

4. Conclusions

The results of the experimental campaign confirm the close interdependence between water retention, shrinkage behaviour, and the evolution of porosity in fibrous peat. The comparison between natural and reconstituted samples highlights the influence of initial fabric, particularly the presence and proportion of inter-ped porosity, on the magnitude and sequence of shrinkage observed during drying. Desaturation-driven shrinkage in natural peat appears to be associated with the drainage of inter-ped voids. In contrast, the reconstituted material, which has a more homogeneous and massive structure, exhibits a predominantly proportional response, more representative of the intra-ped porosity.

The experimental methodology combining shrinkage and water retention measurements enabled a separation of the total void and water ratio into intra- and inter-ped components. The evolution of these components throughout drying suggests a sequential engagement of porosities, where inter-ped voids drain early in the process and intra-ped pores dominate the later stages of shrinkage. This staged behaviour is consistent with the observed transition from desaturation-driven to proportional and accelerated shrinkage.

Mercury intrusion porosimetry provided additional insight into the evolution of the pore size distribution, although limitations in assessing the largest pore sizes remain. Thus, the MIP results were interpreted as being more representative of the intra-ped porosity. The data support the notion of a pore network that shrinks hierarchically, with larger pores reducing at higher water ratios and smaller pores engaging as drying progresses.

Overall, the findings provide further experimental substantiation for a pore-scale framework linking water retention and shrinkage in organic soils. They also emphasise the importance of fabric and pore structure in determining hydraulic and mechanical responses, with implications for the modelling of peat behaviour under varying hydro-mechanical conditions.

The authors gratefully acknowledge Man Xu for providing part of the experimental data.

References

[1]. J. Xu, P. J. Morris, J. Liu, J. Holden, Catena (Amst), **160**, pp. 134–140, (2018)

[2]. G. Kruse, E. D. Haan, *Proceedings of the Second International Workshop on Characterisation and Engineering Properties of Natural Soils*, (2006)

[3]. A. M. Tang et al., Q. J. Eng. Geol. Hydrogeol., 51, **2**, pp. 156–168, (2018)

[4]. N. B. Hobbs, *Q. J. Eng. Geol.* **19**, 7–80 (1986)

[5]. G. Mesri, M. Ajlouni. J. Geotech. Geoenvironmental Eng. **133**, 850–866 (2007)

[6]. J.J.B. Bronswijk, J.J. Evers-Vermeer, Neth. J. Agri. Sci. **38**, 175-194 (1990)

[7]. S. Gebhardt, H. Fleige, R. Horn. J Soils Sediments. **10**, 484–493 (2010),

[8]. X. Peng, R. Horn, Eur J Soil Sci **58**, 98–107 (2007)

[9]. X. Peng, R. Horn, A. Smucker, Soil Sci. Soc. Am. J **71**, 1095-1104 (2007).

[10]. M. Camporese, S. Ferraris, M. Putti, P. Salandin, P. Teatini, Water Resour Res 42, (2006).

[11]. R. Oleszczuk, K. Bohne, J. Szatylowicz, T. Brandyk, T. Gnatowski, J. Plant. Nutr. Soil Sci., 166, 2, pp. 220–224, (2003), doi: 10.1002/JPLN.200390032.

[12]. J. Päivänen, Silva Fennica. **129**, (1973)

[13]. J. S. Price, M. K. Woo, I. Hydrology. J Hydrol (Amst) 103, 275–292 (1988).

[14]. D. P. Ours, D. I. Siegel, P.H. Glaser, J Hydrol (Amst) 196, 348–360 (1997).

[15]. F. Rezanezhad, J. S. Pricem J. R. Craig Can J Soil Sci 92, 723–732 (2012).

[16]. F. Rezanezhad, J.S. Price, W. L. Quinton, B. Lenartz, T. Milojevic, P. V. Cappellen Chem Geol 429, 75–84 (2016).

[17]. H. Zhao, Can. Geotech. J. **60**, 438-452 (2022)

[18]. L.J. Parra-Gómez, S. Muraro, C. Jommi, E3S Web of Conf. **382**, (2023)

[19]. ASTM, D5550-14 *Standard Test Method for Specific Gravity of Soil Solids by Gas Pycnometer* (2014).

[20]. ASTM, D2974-20e1 *Standard Test Methods for Determining the Water (Moisture) Content, Ash Content, and Organic Material of Peat and Other Organic Soils* (2020)

[21]. ASTM, D1997-20 *Standard Test Method for Laboratory Determination of the Fiber Content of Peat and Organic Soils by Dry Mass* (2020)

[22]. UMS, *Operation Manual HYPROP* (2015).

[23]. UMS, *Operation Manual WP4C* (2024).

[24]. H. Yamaguchi, Y. Hashizume, H. Ikenaga, Soils Found., **32**(4), pp. 1–16 (1992)

[25]. H. Yamaguchi, Y. Ohira, K. Kogure, Soils Found., **25**(2), pp. 119–134 (1985).